Plant Physiology and Biochemistry 52 (2012) 38–51

Contents lists available at SciVerse ScienceDirect

Plant Physiology and Biochemistry

journal homepage: www.elsevier.com/locate/plaphy

Research article

Reactive oxygen species from chloroplasts contribute to 3-acetyl-5-isopropyltetramic acid-induced leaf necrosis of *Arabidopsis thaliana*

Shiguo Chen [a,1], Chunyan Yin [a,1], Reto Jörg Strasser [a,b,c], Govindjee [d,2], Chunlong Yang [a], Sheng Qiang [a,*]

[a] *Weed Research Laboratory, Nanjing Agricultural University, Nanjing 210095, China*
[b] *Bioenergetics Laboratory, University of Geneva, CH-1254 Jussy/Geneva, Switzerland*
[c] *North West University of South Africa, South Africa*
[d] *Department of Plant Biology, and Department of Biochemistry, University of Illinois at Urbana-Champaign, Urbana, IL 61801, USA*

ARTICLE INFO

Article history:
Received 22 August 2011
Accepted 2 November 2011
Available online 11 November 2011

Keywords:
3-AIPTA (3-acetyl-5-isopropyltetramic acid)
ROS (reactive oxygen species)
Cell death
Photosynthesis inhibitor
Chlorophyll *a* fluorescence transient
OJIP

ABSTRACT

3-Acetyl-5-isopropyltetramic acid (3-AIPTA), a derivate of tetramic acid, is responsible for brown leaf-spot disease in many plants and often kills seedlings of both mono- and dicotyledonous plants. To further elucidate the mode of action of 3-AIPTA, during 3-AIPTA-induced cell necrosis, a series of experiments were performed to assess the role of reactive oxygen species (ROS) in this process. When *Arabidopsis thaliana* leaves were incubated with 3-AIPTA, photosystem II (PSII) electron transport beyond Q_A (the primary plastoquinone acceptor of PSII) and the reduction of the end acceptors at the PSI acceptor side were inhibited; this was followed by increase in charge recombination and electron leakage to O_2, resulting in chloroplast-derived oxidative burst. Furthermore, the main antioxidant enzymes such as superoxide dismutase (SOD), catalase (CAT) and ascorbate peroxidase (APX) lost their activity. Excess ROS molecules directly attacked a variety of cellular components and subsequently caused electrolyte leakage, lipid peroxidation and cell membrane disruption. Finally, this led to cell destruction and leaf tissue necrosis. Thus, 3-AIPTA-triggered leaf necrosis of Arabidopsis was found to be a result of direct oxidative injury from the chloroplast-originated ROS burst initiated by the inhibition of normal photosynthetic electron transport.

1. Introduction

Reactive oxygen species (ROS), hydroxyl radicals (·OH), singlet oxygen ($^1O_2$), superoxide anions ($O_2^{\bullet -}$) and hydrogen peroxide (H_2O_2), are known to participate in various biotic or abiotic stress responses [1]. A rapid increase in the concentration of ROS (called the "oxidative burst") is a common plant response to various adverse environmental factors, such as pathogen attack and herbicide treatment. Excess intracellular ROS reacts with a large variety of biomolecules, and causes irreversible cellular damage, ultimately leading to plant tissue necrosis. On the other hand, a lower level of ROS might act as a key mediator of programmed cell death and be, thus, used as *signal* molecules leading to disease-related death [2,3].

In plants, oxidative burst triggered by different stresses are attributed to different mechanisms [2]. The major sources of ROS production include photosynthesis in chloroplasts, photorespiration in peroxisomes, mitochondrial respiration, plasma membrane NADPH oxidases and xanthine oxidase, as well as cell wall oxidases and peroxidases [1,2]. The reaction centers of photosystem II (PSII) and photosystem I (PSI) in chloroplasts are considered to be the major generation sites of ROS since they possess an environment

Abbreviations: ABS, photon flux absorption, by photosystem II antenna pigments creating excited chlorophyll molecules; 3-AIPTA, 3-acetyl-4-hydroxyl-5-isopropylpyrroline-2-dione; APX, ascorbate peroxidase; CAT, catalase; CS, optical cross section of the photosynthetic sample; DAB, 3,3′-diaminobenzidine; DCF, dichlorofluorescein; DMTU, dimethylthiourea; ET, energy flux that leads to electron transport beyond Q_A; F_O, F_V, F_M, the initial (minimum), variable and maximum chlorophyll *a* fluorescence intensity; F_J, F_I, chlorophyll *a* fluorescence at the J-step (2 ms) and at the I-step (30 ms) during fluorescence transient; FDA, fluorescein diacetate; H_2DCF-DA, dichlorofluorescin diacetate; MDA, malondialdehyde; NAC, *N*-acetyl-L-cysteine; NBT, nitroblue tetrazolium; PS I, photosystem I; PS II, photosystem II; Q_A, Q_B, PSII primary and secondary plastoquinone electron acceptors; R_J, number of PSII RCs with Q_B-site filled by PSII inhibitor; RC, reaction center; RE, reduction of end accepters at the PSI electron accepter side; ROS, reactive oxygen species; SOD, superoxide dismutase; TBA, thiobarbituric acid; TBD, Trypan Blue D; TR, energy flux trapping (leading to Q_A reduction) by all the PSII reaction centers; φ_{Po}, the maximum quantum yield of primary PSII photochemistry; ψ_{Eo}, the probability that a trapped exciton moves an electron into the electron transport chain beyond Q_A; φ_{Eo}, the maximum quantum yield for PSII electron transport; φ_{Ro}, the quantum yield for the reduction of the end electron acceptors at the PSI acceptor side; δ_{Ro}, the probability with which an electron from the intersystem electron carriers is transferred to reduce the end electron acceptors at the PSI acceptor side.

* Corresponding author. Tel./fax: +86 25 84395117.
E-mail address: wrl@njau.edu.cn (S. Qiang).

[1] Authors contributed equally to this work.

[2] G. contributed mainly in the discussion and in the writing of the paper, but not in the experiments.

0981-9428/$ – see front matter © 2011 Elsevier Masson SAS. All rights reserved.
doi:10.1016/j.plaphy.2011.11.004

rich in oxygen, reductants, and high-energy intermediates [4]. A complex array of ROS can be generated in chloroplasts resulting from the accumulation of $^1O_2$ when the absorption of light energy exceeds the capacity for CO_2 assimilation or leads to inactivation of PSII reaction centers (RCs) and from the production of $O_2^{\bullet -}$ due to the photoreduction of oxygen at PSI at high light intensities [5].

Reactive Oxygen Species are formed in chloroplasts when plants are treated with herbicides, inhibitors of photosynthesis. Bipyridinium herbicides such as paraquat and diquat, commonly used in agronomy, exert their herbicidal activity by replacing $NADP^+$ that is the normal ultimate electron acceptor of PSI. When plants are exposed to sunlight, these herbicides accept electrons from PSI and pass them to oxygen leading to the generation of $O_2^{\bullet -}$ [6]. The reduced photosynthetic electron acceptors of PSI enhance the reduction of O_2, which results in subsequent formation of $O_2^{\bullet -}$, H_2O_2 and $\cdot OH$ [7,8]. Several other herbicides, such as diuron, atrazine, bentazon, bromoxynil, and hexazinone, are PSII herbicides which cause chloroplastic oxidative burst and severe oxidative stress [9]. Additionally, diphenyl ether (e.g. lactofen) and protoporphyrinogen oxidase-inhibiting herbicides can induce generation of $^1O_2$ in intact illuminated thylakoids; this is related to the formation of protoporphyrin IX, which results in oxidative damage of the extensive membrane system of the thylakoids [10]. In the case of some other photosynthesis-inhibiting herbicides, their primary toxic mechanism is to block the photosynthetic electron chain, which is followed by ROS generation, oxidative damage and cell death [9]. Hence, knowledge of the mechanism of ROS generation and toxicity is very important for research and development of new photosynthesis herbicides.

Tetramic acid (pyrrolidine-2,4-diones ring system, Fig. 1 (1)) is a recurrent motif among natural products originating from a variety of marine and terrestrial species [11]. The family of this compound continues to attract a great deal of interest because of broad range of desirable biological and pharmaceutical activities. Some tetramic acid moieties, such as 3-benzoyl-pyrrolidin-2,4-dion-derivates [12] and 2-ethyl-4,6-dimethyl-phenyl-substituted tetramic acid derivates [13], have been found to possess unusual physiological activity and been patented for herbicidal use. A most frequently used compound is 3-acyl-tetramic acid; it is also pharmacologically most interesting due to its structural simplicity and high biological activity [14]. One of the best representative natural metabolites of this family is tenuazonic acid (Fig. 1(2)). A previous study has revealed that tenuazonic acid is a novel type of photosynthesis inhibitor [15], which causes cell necrosis attributed to direct oxidative damage from the chloroplast-derived ROS burst [16]. It has the potential to be developed as a new bioherbicide since it has a wide range of herbicidal activities [16]. 3-Acetyl-5-isopropyltetramic acid (3-AIPTA) (Fig. 1(3)) is another very interesting 3-acyl-tetramic acid derivate, which has been isolated from a microorganism *Alternaria tenuis* [17]. The side chain of 3-AIPTA at the 5-position of pyrrolidine-2,4-diones ring is an isopropyl group different from a sec-butyl group of tenuazonic acid. Thus, 3-AIPTA is another good tool besides tenuazonic acid for the investigation of the structural and biological characteristics of photosynthetic organisms, as well as for the mode of action of tetramic acid families. However, till now there have been very few reports on 3-AIPTA effects. Our previous studies revealed that 3-AIPTA and some of its analogues inhibit PSII electron transport rate in algal cells as well as their growth [15]. Based on bioassay results, 3-AIPTA is shown to be phytotoxic in a wide range of plants, from weeds to crops (Supplementary Table 1). Further, it kills seedlings of both mono- and dicotyledonous weeds. 3-AIPTA was shown to inhibit both PSII and PSI electron transport activity, as well as root and shoot length of seedlings. 3-AIPTA strongly interrupts electron flow beyond Q_A by binding to the D1 protein. However, it has a different binding behavior during interaction with the D1 protein as compared to that known for 'classical' PSII inhibitors [18]. At high concentrations, 3-AIPTA inhibits the reduction of the end electron acceptors on the PSI acceptor side [18]. However, the mode of action of leaf necrosis induced by 3-AIPTA is still unknown.

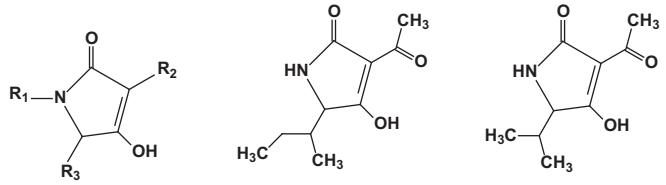

Tetramic acid (**1**) Tenuazonic acid (**2**) 3-AIPTA (**3**)

Fig. 1. The structure of tetramic acid (1), tenuazonic acid (2) and 3AIPTA (3).

In this paper, we show that during leaf necrosis of *Arabidopsis thaliana,* 3-AIPTA leads to a chloroplast-derived ROS burst under illumination; subsequently, ROS causes irreversible oxidative damage and ultimately cell death. We found that the inhibition of the PSII electron transport beyond Q_A and the reduction of end electron acceptors on the PSI acceptor side is an earlier event than the ROS burst. Based on this evidence, it is suggested that the ROS generation in the chloroplast results from the blockage of the photosynthetic electron transport, which plays an important role in 3-AIPTA-induced cell necrosis.

2. Results

2.1. 3-AIPTA induces lesion formation in Arabidopsis leaves

When detached-intact *A. thaliana* leaves are treated with 500 μM 3-AIPTA for 0–96 h under illumination, visible lesions are clearly observed (Fig. 2A). Usually, macroscopic water-soaked lesions begin to appear after 48 h treatment, with the tissues turning brown; then, these lesions spread, and eventually become necrotic by 96 h (Fig. 2A). The 3-AIPTA-elicited lesions led to cell death, as shown by Trypan Blue staining, and by ion leakage (an indicator of plasma membrane damage); the ion leakage started to increase after 24 h treatment with 3-AIPTA, suggesting that membrane destruction had occurred (Fig. 2C). At this time, a portion of the cells began to die (data not shown). After 30 h of 3-AIPTA treatment, almost all the cells had died, and ion leakage had increased to a very high level (Fig. 2B and C). This pattern is essentially the same as for the injury of leaf tissues caused by photosynthesis-inhibiting herbicide bentazon.

2.2. Histochemical location determines 3-AIPTA-induced oxidative burst

To determine whether reactive oxygen species are involved in cell necrosis of Arabidopsis leaves in the above-described experiments, 3,3′-diaminobenzidine (DAB) and nitroblue tetrazolium (NBT) were used to stain the samples in order to check the in situ accumulation of H_2O_2 and $O_2^{\bullet -}$ in intact illuminated leaves treated with 500 μM 3-AIPTA. DAB polymerizes and turns deep brown in the presence of H_2O_2 and the intensity of coloration and its location can be quantitatively assessed and photographed [19]. The development of the DAB-H_2O_2 reaction product in intact leaves in response to 3-AIPTA or bentazon treatment is shown in Fig. 3A. No visible H_2O_2 accumulation was observed in controls after 6 h. However, H_2O_2 was detected as early as 1 h in leaves treated with 3-AIPTA or bentazon, with the color continuing to darken with incubation over a 6 h period. The microscopic examination of leaf

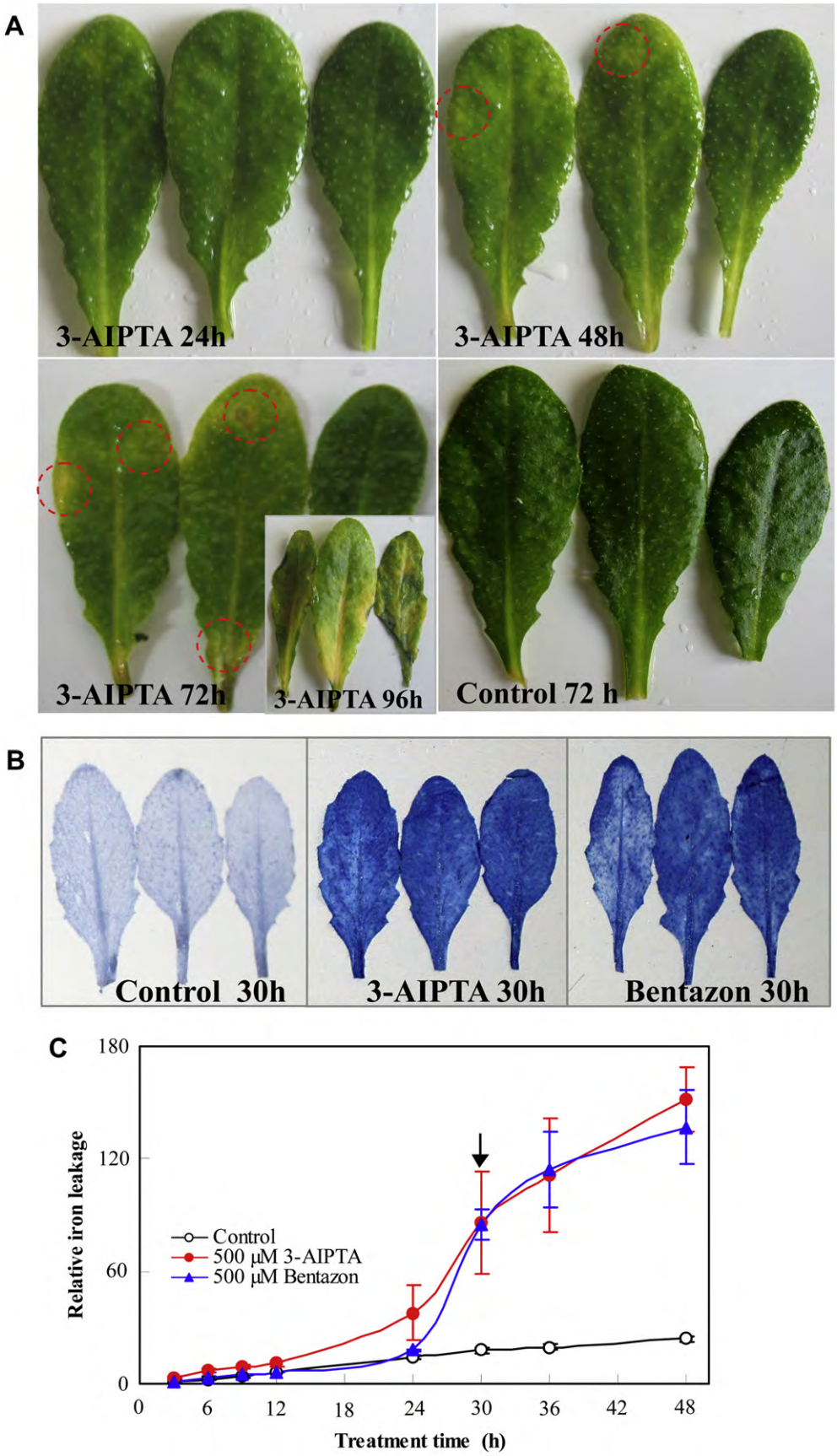

Fig. 2. Cell death-associated symptoms induced by 3-AIPTA or bentazon. *A. thaliana* leaves or leaf discs were vacuum infiltrated with 500 µM 3-AIPTA or 500 µM bentazon for the indicated times under illumination. (A) Progression of necrotic symptoms in detached-intact leaves induced by 3-AIPTA. Red circles indicate leaf lesions showing a brown leaf-spot. (B) cell death at 30 h after 3-AIPTA or bentazon treatment. Leaves were stained with Trypan blue D. (C) ion leakage was determined, as described in materials and methods, and reported as the ratio of the value measured in 3-AIPTA- or bentazon-treated samples to the value obtained in distilled water-treated samples (control) at 3 h; raw value of water-treated samples at 3 h is 6.38 ± 0.93 µS cm^{-1}. The arrow indicates the time at which cell death was tested. (For interpretation of the references to colour in this figure legend, the reader is referred to the web version of this article.)

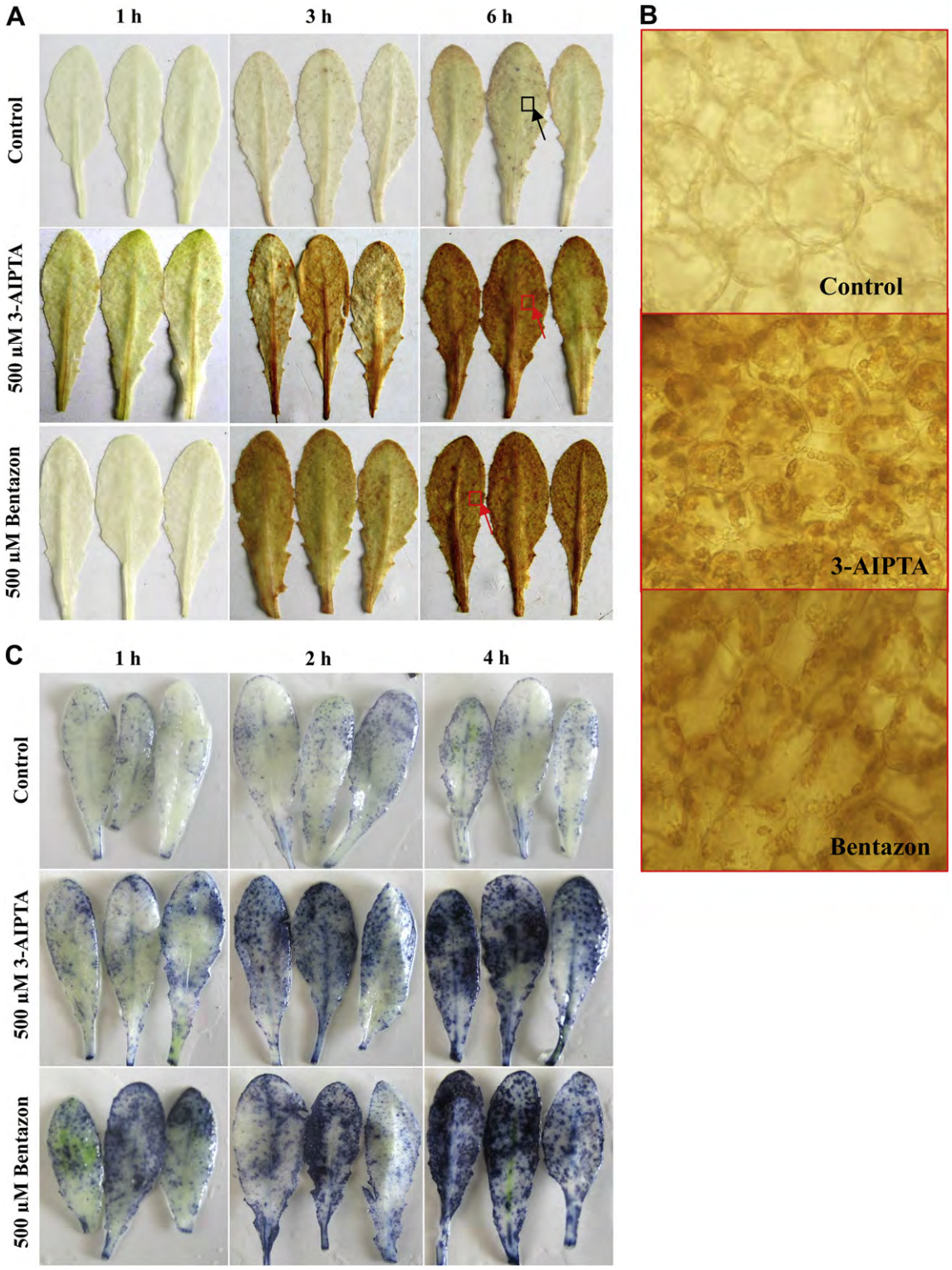

Fig. 3. The induction of ROS generation at the leaf level after 3-AIPTA or bentazon treatment. The detached intact-leaves of *A. thaliana* were treated with distilled water (control) or with 500 μM 3-AIPTA or 500 μM bentazon for the indicated time under illumination. Experiments were repeated at least four times with similar results. (A) histochemical detection of H_2O_2 with DAB staining. The square box sections of DAB-stained leaves were tested under the microscope. (B) microscopic observation of H_2O_2 production. The images were taken at 600× magnification. H_2O_2 generation originates from chloroplasts after 3-AIPTA treatment or bentazon (the site observed under microscope is indicated by red square boxes and arrows in Fig. 3A). No oxidized DAB deposit was observed in the chloroplasts of control (the site observed under microscope is indicated by a black square box and an arrow in Fig. 3A). (C) histochemical detection of $O_2^{\bullet -}$ generation with NBT staining. (For interpretation of the references to colour in this figure legend, the reader is referred to the web version of this article.)

cells showed that oxidized DAB deposits were mostly located in the chloroplasts (Fig. 3B). Since H_2O_2 was detected in chloroplasts, $O_2^{\bullet -}$ production must have taken place in the chloroplasts since $O_2^{\bullet -}$ is known to be rapidly converted to H_2O_2 by SOD. Intracellular $O_2^{\bullet -}$ generation can be detected using dark-blue insoluble formazen produced by the reaction of NBT and $O_2^{\bullet -}$ [8,20]. A similar result was observed in leaves treated with 3-AIPTA or bentazon (Fig. 3C). Little NBT staining was observed in controls. Treatment with 3-AIPTA or bentazon for 1 h led to slight accumulation of $O_2^{\bullet -}$ in the leaf tissues. The color was very dark in intact leaves treated with 3-AIPTA or bentazon for 4 h, and then it became lighter. These results reveal that large amount of ROS is generated in the cells of leaves treated with 3-AIPTA. Thus, we conclude that chloroplasts are a major source of ROS production. This was confirmed by experiments with dichlorofluoresc in diacetate (H_2DCF-DA) (see below).

2.3. Dichlorofluorescein measures 3-AIPTA-induced ROS production in mesophyll cells

Dichlorofluorescein (DCF) has been used to visualize oxidative processes in plants in response to various stresses [21,22]. In order to visualize intracellular ROS formation in cells, H_2DCF-DA was used in our studies. After epidermis-less leaf segments were treated with 500 μM 3-AIPTA or bentazon for 0 to 3 h, ROS production was observed in mesophyll cells (see time course in Fig. 4A). A rapid increase of green DCF fluorescence signal in leaf segments treated with 3-AIPTA or bentazon for 15 min was observed, reaching a peak at 60 min. Beyond 1 h after treatment, the DCF fluorescence intensity began to decline, and then decreased to the control level at 3 h (Fig. 4A). Interestingly, DCF fluorescence signals were first found in the chloroplasts of mesophyll cells within 15 min (data not shown). By 30 min of 3-AIPTA or bentazon incubation, DCF signals were still mainly localized in the chloroplasts of mesophyll cells (Fig. 4B). However, by 1 h, DCF signals dramatically increased and dispersed through the cell when mesophyll cells were incubated with 3-AIPTA for 1 h (Fig. 4B). These results indicate that ROS is generated in the chloroplast of 3-AIPTA- or bentazon-treated leaf segments, which over time diffuses out of the chloroplasts and cells into the surrounding cells. ROS scavengers *N*-acetyl-L-cysteine (NAC), dimethylthiourea (DMTU), CAT and SOD significantly suppressed ROS levels in mesophyll cells treated with 3-AIPTA or bentazon (Fig. 4C). Although exogenously added CAT only remains in the apoplast, intracellular generated ROS can leave the cells as H_2O_2 and enter other cells via an apoplastic route. A similar phenomenon has been found in the O_3-induced oxidative burst [21,22]. Our results clearly demonstrate that 3-AIPTA treatment causes chloroplast-derived oxidative burst in Arabidopsis mesophyll cells.

The ideas, discussed above, were further confirmed by data obtained from mesophyll protoplast experiments. When 3-AIPTA was added to H_2DCF-DA preloaded protoplasts, DCF fluorescence signal gradually intensified during 10 min treatment of protoplasts with 3-AIPTA, as observed by confocal microscopy (see Supplementary *Movie 1*). In contrast, DCF signals of control protoplasts always remained at very low levels over the same time period (Supplementary *Movie 2*). In an attempt to identify the source of ROS, both chloroplast autofluorescence (red) and DCF fluorescence (green) of mesophyll cells, treated with 500 μM 3-AIPTA for 10 min, were measured simultaneously. The green DCF signals exactly match that of the red chloroplast autofluorescence signals, showing a single yellow image when the red chloroplast fluorescence was overlaid with the green DCF signals (Fig. 4D). Thus, we conclude that the primary site of 3-AIPTA-induced ROS burst in mesophyll cells is the chloroplast.

Supplementary data associated with this article can be found, in the online version, at doi:10.1016/j.plaphy.2011.11.004.

2.4. Effect of 3-AIPTA on antioxidant enzymes

In order to examine the contribution of antioxidant enzymes in ROS production and in the protection of cells against oxidative stress, we tested the activities of several important antioxidant enzymes such as SOD, CAT and APX in epidermal-less Arabidopsis leaf segments under 3-AIPTA treatment (Fig. 5). A significant decrease in the activities of SOD (Fig. 5A) and APX (Fig. 5B) occurred within 4 h of treatment. However, the CAT activity showed a marked decline even after just 1 h (Fig. 5C). After 6 h of treatment, the activities of SOD, APX and CAT decreased by 56%, 65%, and 73% respectively, compared to the control. Moreover, the decrease of activities of these antioxidant enzymes is a later event relative to 3-AIPTA-induced chloroplast-derived ROS burst. However, if the enzyme extracts were treated directly with 3-AIPTA, 3-AIPTA itself had no significant effect on the activities of SOD, CAT and APX (Supplementary Figure 1). This implies that in leaf tissues, the 3-AIPTA-induced ROS burst had destroyed the antioxidant enzyme system.

2.5. 3-AIPTA-triggered cellular damage is associated with chloroplast-derived ROS burst

To further investigate the influence of 3-AIPTA-induced ROS on cellular structure and function, we monitored cell viability of mesophyll cells following 3-AIPTA treatment. The loss of cell viability is reflected in a loss of fluorescein diacetate (FDA) fluorescence. As shown as Fig. 6A, the FDA fluorescence signal dramatically decreased relative to the control after mesophyll cells were treated for 3 h with 500 μM bentazon. Within 3 h of 500 μM 3-AIPTA treatment, only a slight decrease in FDA signal was observed. However, after 6 h of 3-AIPTA or bentazon incubation, FDA fluorescence decreased to a very low level and became negligible (Fig. 6A, B). ROS scavengers NAC, DMTU, CAT and SOD suppressed the 3-AIPTA-induced damage to cell viability (Fig. 6C). Thus, we conclude that chloroplast-derived oxidative burst plays an important role during 3-AIPTA-triggered cell death and leaf tissues necrotic lesion.

The loss of cell viability may indicate that 3-AIPTA-treatment destroys plasma membranes where lipids exist since lipids are particularly sensitive to ROS produced during environmental stress. Thus, the toxicity of ROS has often been monitored by measuring lipid peroxidation as malondialdehyde- (MDA-) reactive products. In order to test the influence of 3-AIPTA-induced ROS on membranes and lipids, we measured changes in ion leakage and lipid peroxidation in cells treated with 3-AIPTA, combining it with ROS scavenger treatment. Pretreatment with NAC, DMTU, CAT and SOD significantly suppressed 3-AIPTA-caused ion leakage (Fig. 6D) and lipid peroxidation (Fig. 6E) in leaf discs incubated with 500 μM 3-AIPTA for 30 h, but this did not completely prevent the damage. This indicates that 3-AIPTA-caused damage of membrane structure and lipids was, in all likelihood, due to 3-AIPTA-induced chloroplast-derived ROS production.

2.6. Inhibition of photosynthetic electron flow precedes 3-AIPTA-induced ROS burst

Based on the known action and injury symptoms, 3-AIPTA appears to be similar to commercial photosynthesis inhibitor herbicides such as bentazon, atrazine and diuron. 3-AIPTA interrupts PSII electron transport from Q_A to Q_B (where Q_A is the primary and Q_B is the secondary plastoquinone acceptor of PSII); it is suggested to act

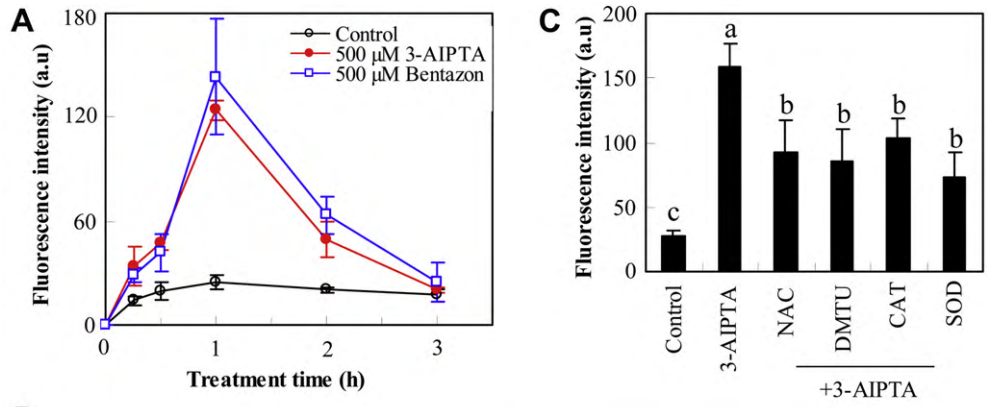
A
Fluorescence intensity (a.u)
180
120
60
0
0
1
2
3
Treatment time (h)
Control
500 μM 3-AIPTA
500 μM Bentazon
C
Fluorescence intensity (a.u)
200
150
100
50
0
a
b
b
b
b
c
Control
3-AIPTA
NAC
DMTU
CAT
SOD
+3-AIPTA

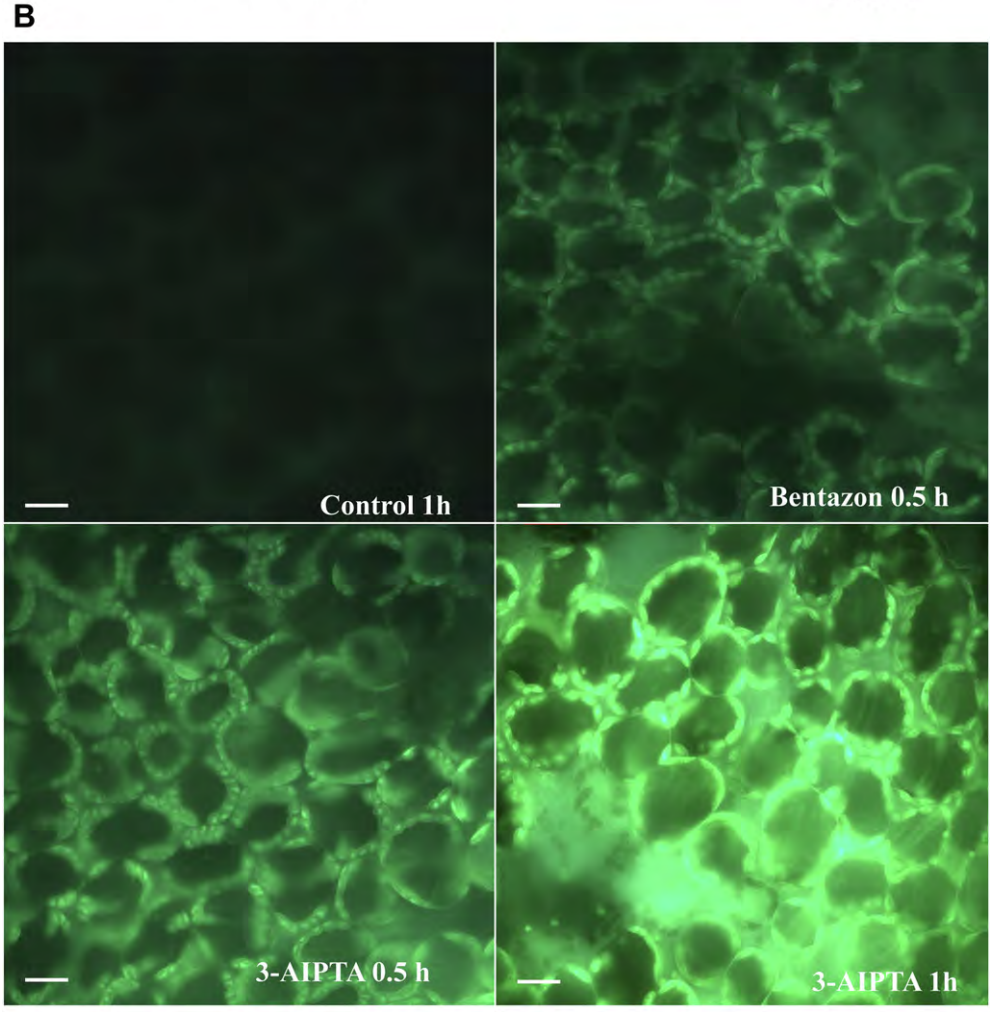
B
Control 1h
Bentazon 0.5 h
3-AIPTA 0.5 h
3-AIPTA 1h

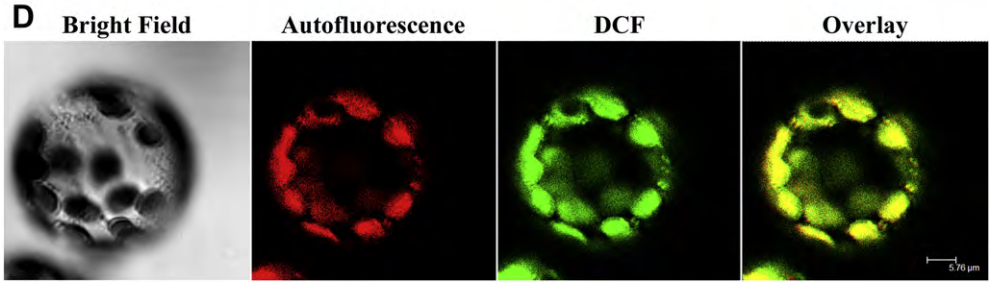
D
Bright Field
Autofluorescence
DCF
Overlay

by binding to the Q_B-site on the D1 protein [18]. To examine the role of photosynthesis inhibition in the formation of 3-AIPTA-induced chloroplast-derived ROS, we simultaneously measured, although indirectly, the photosynthetic activity of 3-AIPTA-treated epidermis-less leaf segments by the fast Chl *a* fluorescence rise, the OJIP transient, and ROS generation. It is well known that Chl *a* fluorescence transient is a non-invasive, efficient, rapid and sensitive tool to probe the state of the structure as well as function of the photosynthetic apparatus [23,24, and references therein]. In Fig. 7A and B, the chlorophyll *a* fluorescence transients of the untreated leaf segments (control) and those treated with 500 μM 3-AIPTA for 5–120 min are shown. With increasing treatment time, the largest change in the OJIP fluorescence transient is in the increase in the rate of rise from the O to the J-step; the F_J (2 ms) becomes equal to the F_M (maximum fluorescence). An increase in the J-level is attributed to the faster accumulation of Q_A^-; this occurs because of interruption of electron flow beyond Q_A [23,24].

To evaluate the effect of 3-AIPTA on the IP phase, the thermal phase, of the fluorescence induction curve OJIP, two different normalization procedures were used (Fig. 7C and D). When the leaf segments are treated with 3-AIPTA for 5–120 min, the amplitude of the IP phase is strongly but not completely reduced. The IP phase is related to electron transfer through PSI and the traffic jam of electrons caused by a transient block on the acceptor side of PSI possibly due to the inactivation of ferredoxin-NADP+-reductase (FNR) [25], and references therein].

The OJIP fluorescence transients were also analyzed by the JIP-test to deduce 6 structural and functional parameters. In Fig. 8A, no change in the maximum yield of primary photochemistry ($\varphi_{Po} = TR_0/ABS = F_v/F_M$; see the list of abbreviations) was found until 30 min of 3-AIPTA treatment. By 60 min, 3-AIPTA treatment caused a significant decrease of φ_{Po}, compared to water-treated leaf segments (control) (Fig. 8A). Since PSII electron flow beyond Q_A was blocked, φ_{Eo}, which expresses maximum quantum yield of PSII electron transport further than Q_A^-, had a sharp decrease as early as 5 min of 3-AIPTA treatment (Fig. 8B). If the Q_A^- cannot be reoxidized in time, a large accumulation of Q_A^- is expected to increase the concentration of inactive PSII RCs. As the treatment time of 3-AIPTA was increased, PSII RCs were further inactivated, exhibiting an approximately linear, and significant, increase of the amount of non-Q_A reducing RCs (Fig. 8C): after 5 min of 3-AIPTA incubation of leaf segments, the amount of non-Q_A reducing RCs had increased 130% relative to the control; by 60 min and 90 min, about 40% and 61% of PSII RCs were inactivated. Other evidence has indeed also suggested that PSII inhibitors result in inactivation of PSII RCs when the electron transport from Q_A to Q_B is blocked by the herbicide occupying the Q_B-site [see e.g., 23,24]. Our data suggest that 3-AIPTA-caused severe closure of PSII RCs should be attributed to an enhancement of the R_J parameter, which reflects the number of PSII RCs with the Q_B-site filled with 3-AIPTA (Fig. 8D).

The effects of 3-AIPTA on two parameters related to step-I, φ_{Ro} expressing the quantum yield for the reduction of the end electron acceptors at the PSI acceptor side, and RE_0/CS reflecting electron flux to the end electron acceptors at the PSI acceptor side, are shown in Fig. 8E and F. At shorter 3-AIPTA treatment time (under 30 min), insignificant changes in the values of φ_{Ro} and RE_0/CS were found. However in the case of 3-AIPTA treatment for longer time (over 30 min), the φ_{Ro} level and the RE_0/CS level showed a distinct decrease. Such results indicate that 3-AIPTA has a visible effect on electron flow at the PSI acceptor side. Obviously, the inhibition of photosynthetic electron transport is an earlier event than chloroplast-derived ROS burst during 3-AIPTA-triggered cell necrosis. Thus, there must be a series of events that lead from the effects on the electron flow to the production of ROS that damages the system.

3. Discussion

3.1. 3-AIPTA-triggered leaf lesion is a consequence of oxidative damage

Our data on DAB and NBT staining reveals that 3-AIPTA treatment leads to accumulation of H_2O_2 and $O_2^{\bullet -}$ within the leaves, and this leads to leaf necrosis (Figs. 2 and 3). After intact leaves were treated with 3-AIPTA for several hours, 3-AIPTA-induced ROS in cells increased to the highest level (Fig. 3A, C). However, by 30 h of 3-AIPTA treatment, a significant electrolyte leakage took place as a result of plasma membrane damage. At this point in time, almost all the leaf cells die (Fig. 2B, C). At 48 h, leaves showed clear physiological damage due to turgor loss and tissue collapse (Fig. 2A). Based on the analysis of the time of ROS generation and cell necrosis, it is evident that 3-AIPTA-induced ROS overproduction occurs before cell membrane disruption which preceeds cell necrosis. This conclusion is corroborated by evidence from DCF staining experiments, which showed that under illumination, 3-AIPTA treatment causes a distinct increase of ROS generation in mesophyll cells within 1 h (Fig. 4A and B). This mode of action and the injury symptoms are the same as that of a photosynthesis inhibitor herbicide bentazon ([26], Figs. 2 and 3).

Photosynthesis-inhibiting herbicides can be divided into two distinct groups, PSII inhibitors and PSI inhibitors. Both block the synthesis of ATP and NADPH, followed by ROS generation, oxidative damage and ultimately cell death [9]. When photosynthetic systems are exposed to light, PSI inhibitor herbicides become active and form ROS, which readily cause lipid peroxidation and chlorophyll breakdown [9]. This destroys cell membrane integrity, so that the cells and the organelles “leak”, leading to rapid leaf wilting and desiccation, and eventually to plant death [7,9,10]. PSII inhibitor herbicides are known to interrupt electron flow beyond Q_A by binding to the D1 protein at the Q_B-site in the PSII reaction center. This blockage stops photosynthesis, leading to a large amount of ROS production in chloroplasts, especially $^1O_2$ [27,28]. These ROS molecules disrupt cell membranes and cause chloroplast swelling, membrane leakage, and ultimately cellular destruction and plant necrosis. 3-AIPTA, which as a photosynthesis inhibitor, induced a chloroplast-derived ROS burst (Figures 3B, 4B and D; Supplementary Movies 1, 2); and this is responsible for 3-AIPTA-triggered cell death and necrotic leaf lesions.

Reactive oxygen species normally exist in all aerobic cells in balance with biochemical antioxidants. Oxidative stress, and as

Fig. 4. Production and intracellular localization of ROS in *A. thaliana* mesophyll cells after 3-AIPTA or bentazon treatment. The epidermis-less leaf segments or mesophyll protoplasts were treated with distilled water (control), 500 μM 3-AIPTA- or bentazon for the indicated times. (A) time course of change in DCF fluorescence intensities from images of 3-AIPTA- or bentazon-treated illuminated mesophyll cells. (B) DCF fluorescence images of mesophyll cells at the indicated times. Bar = 25 μm. (C) effect of ROS scavengers on 3-AIPTA-induced ROS generation in mesophyll cells. Mesophyll cells were pretreated with either NAC (1 mM) or DMTU (1 mM) or CAT (300U/mL) or SOD (400U/mL) for 2 h, subsequently incubated with 500 μM 3-AIPTA for 1 h under illumination. Data are presented as means ± SD ($n = 5$). Means denoted by the same letter did not significantly differ at $p < 0.05$. (D) intracellular localization of ROS in 3-AIPTA-treated mesophyll protoplasts. Protoplasts-preloaded with H_2DCF-DA were treated with distilled water (control) or 500 μM 3-AIPTA for 10 min, and observed by a confocal microscope. Green signals indicate GFP of DCF. Red signals indicate chloroplast autofluorescence. Note that the localization of the green fluorescence (DCF) signals matched that of the red fluorescence (autofluorescence) signals, showing a single yellow image. Green signals were not found in the outer membrane of chloroplasts. This experiment was repeated at least three times with similar results. Bar = 5.76 μm. (For interpretation of the references to colour in this figure legend, the reader is referred to the web version of this article.)

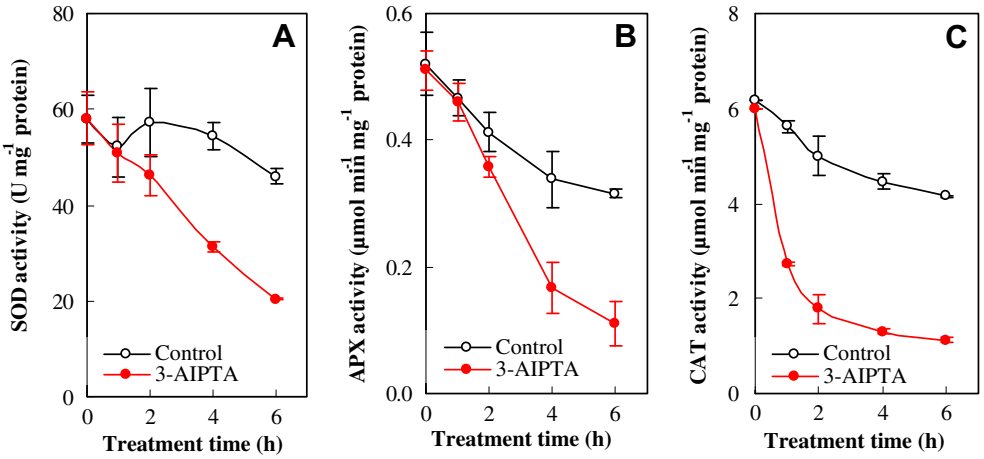

Fig. 5. Time course of changes in the activities of antioxidant enzymes SOD (A), APX (B) and CAT (C) in the epidermis-peeled leaf segments of *A. thaliana* exposed to 3-AIPTA. Data are presented as means ± SD ($n = 4$).

a consequence cellular damage, occurs when this critical balance is disrupted due to a ROS burst, antioxidant depletion, or both [29]. To protect against this cellular damage caused by ROS, it is absolutely essential for plants to make use of antioxidant enzymes. SOD converts superoxide anion $O_2^{\bullet -}$ into a less toxic product, namely H_2O_2 and O_2. Two of the major enzymatic scavengers of H_2O_2 are CAT and APX [30]. Our present data show that 3-AIPTA treatment not only induces ROS overproduction but also destroys the antioxidant enzyme system of mesophyll cells of Arabidopsis (Fig. 5). In the case of the loss of the activity of antioxidant enzymes such as SOD, CAT and APX, ROS molecules are expected to react with a variety of cellular components and then cause irreversible damage that results in the oxidative destruction of the cells [2]. In a cell, the main risk produced by H_2O_2 and $O_2^{\bullet -}$ comes from the generation of ·OH radicals, which is the most toxic of all ROS. The ·OH radical directly attacks most biomolecules, such as amino acids, membrane lipids and organic acids; this causes damage at site-specific points on account of very short life of ·OH, so that the cells and organelles "leak", leading to irrepairable metabolic dysfunction and cell death, and eventually to leaf wilting and desiccation [9]. $^1O_2$ is more reactive than H_2O_2 and $O_2^{\bullet -}$, which can also react directly with many biomolecules accompanied by chlorophyll breakdown and lipid peroxidation. Finally, these events result in the destruction of membrane integrity and loss of cell function. As a result, the formation of other ROS could be stimulated, which could cause further severe damage of cells [31]. Previous investigations have suggested that $^1O_2$ is an important damaging species during photoinhibition caused by stress such as high light or PSII herbicide treatment [27]. It is very clear that 3-AIPTA treatment caused severe oxidative damage of mesophyll cells, such as the loss of cell viability, cell membrane rupture, ion leakage and lipid peroxidation (Fig. 6). ROS scavengers can significantly suppress these damages because ROS generation is an earlier event than the injury of mesophyll cells. This suggests that ROS production injures cellular components through lipid peroxidation and oxidative damage.

Based on the above results, chloroplast-originated ROS burst plays an important role during 3-AIPTA-triggered cell death and leaf tissue necrotic lesion.

3.2. 3-AIPTA-induced chloroplast-derived ROS burst is attributed to the inhibition of electron transport in photosynthesis

The experimental results of histochemical staining showed that chloroplasts were a major source of 3-AIPTA-induced ROS production (Figures 3B, 4B and D). Like bentazon, in the early stage of 3-AIPTA treatment, DCF fluorescence signal produced by ROS was observed only within the chloroplasts in mesophyll cells, and then it diffused out of the chloroplast into cytoplasm, and even into intercellular spaces (Fig. 4B). This means that the primary site of 3-AIPTA-induced ROS generation in mesophyll cells is the chloroplast.

In the chloroplasts, the major generation site of ROS is PSI and PSII [4]. When photosynthetic electron transport chain is overreduced, $^1O_2$ is continuously produced by PSII [2,8]. Moreover, $^1O_2$ generation in photoinactivated PSII centers is directly correlated with photoinhibition [8]. As a PSII inhibitor, 3-AIPTA inhibits electron flow beyond Q_A by binding to the Q_B-site ([18]; Fig. 7A and B and Fig. 8B and D). Once the forward electron transport cannot proceed, Q_A will be overreduced, causing an accumulation of Q_A^- and the ensuing closure of PSII RCs (Figs. 7B and 8C). The overreduction of Q_A on the PSII acceptor side results in thylakoid overenergization and thus increases the energy available for the charge recombination reaction. This can lead to the formation of chlorophyll triplet state (^{3}Chl), which in turn, reacts with O_2 to form $^1O_2$ and generates other toxic ROS [4,27,28,32]. Prior studies have suggested that the reduction of O_2 is the starting point for a series of reactions leading to ROS generation on the PSII electron acceptor side [33]. $O_2^{\bullet -}$ molecules are generated by PSII via electron transport to O_2 under reducing conditions. Experiments show that $Pheo^-$ and Q_A^- and Cyt b_{559} and reduced Q_B can serve as reductants for O_2 [28,33]. Further reduction of $O_2^{\bullet -}$ within PSII is expected to produce other two reactive oxygen species such as H_2O_2 and ·OH [4]. It has been proposed that H_2O_2 is formed by dismutation of $O_2^{\bullet -}$ known to occur either spontaneously or by catalysis using endogenous SOD, as well as by the interaction of $O_2^{\bullet -}$ with a PSII metal center [33]. ·OH is formed in illuminated PSII membranes through the reduction of H_2O_2 via the Fenton reaction [33]. Recently, the production of ·OH has been demonstrated in the presence of either phenolic- or urea-type photosynthetic herbicides [28].

However, the major mechanism of $O_2^{\bullet -}$ production in chloroplasts is by the reduction of O_2 by PSI [4,32,34]. Further reduction of $O_2^{\bullet -}$ within the cell produces the other two ROS: H_2O_2 and ·OH [4]. SOD in chloroplast can convert $O_2^{\bullet -}$ into H_2O_2 [4]. In the presence of transition metal ions such as Fe and Cu, H_2O_2 and $O_2^{\bullet -}$ can react and form ·OH [2,9]. Additionally, highly reduced photosynthetic electron carriers would enhance reduction of O_2 by PSI, which results in subsequent formation of $O_2^{\bullet -}$, H_2O_2 and ·OH [5,7,8]. A smaller I–P amplitude during chlorophyll a fluorescence transient

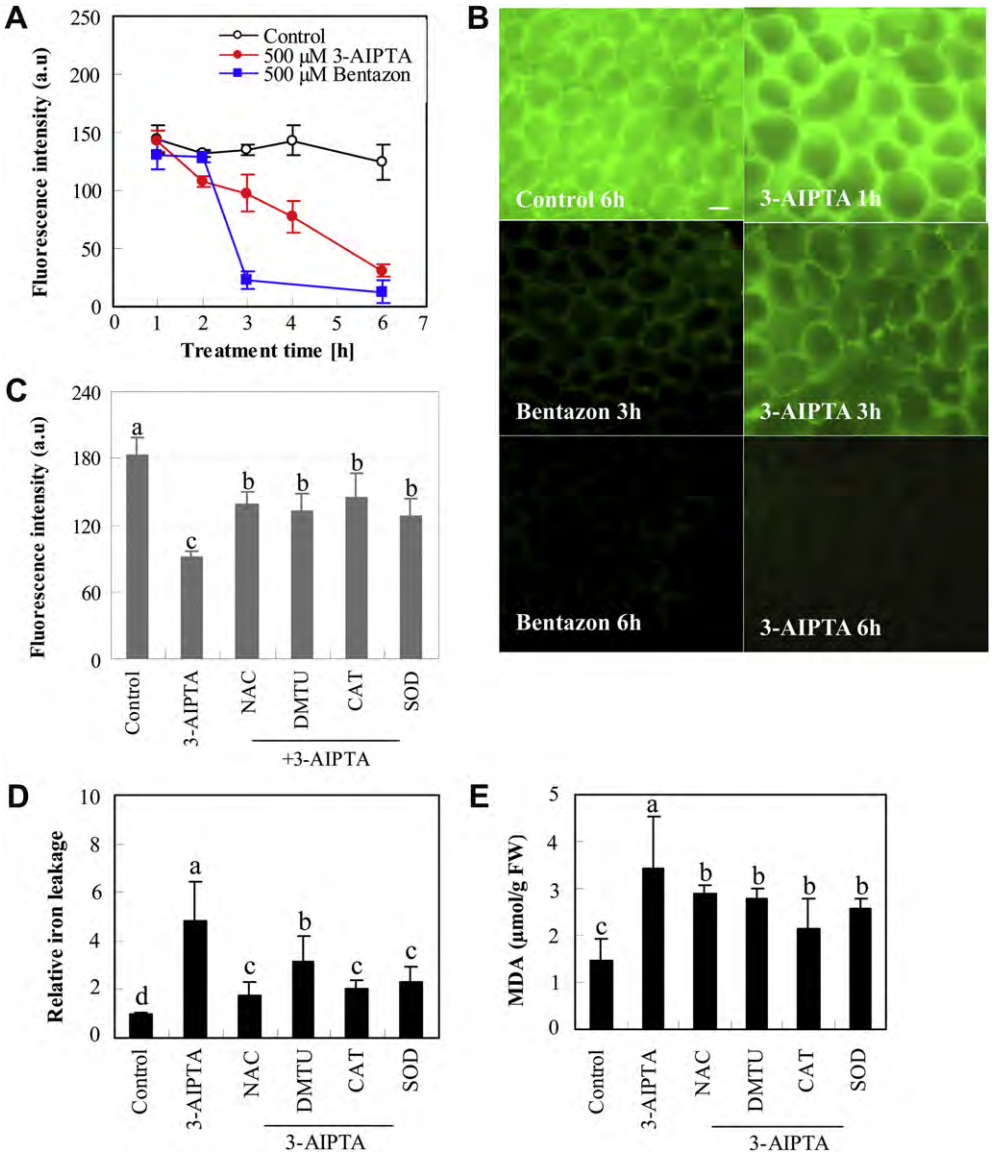

Fig. 6. Effect of 3-AIPTA on cell viability (A–C) and cellular membrane (D–E) during 3-AIPTA- or bentazon-induced cell death. Epidermis-less leaf segments of *A. thaliana* were treated with distilled water (control), 500 μM 3-AIPTA or 500 μM bentazon for the indicated times under illumination. After treatment, segments were collected and stained with 0.01% FDA before microscopic observation. Similar results were repeated three times. (A) time course of change in FDA fluorescence intensities from images of control and 3-AIPTA- or bentazon-treated mesophyll cells. (B) FDA fluorescence images of control or 500 μM 3AIPTA- or 500 μM bentazon-treated mesophyll cells at the indicated times. Bar = 20 μm. (C) mesophyll cells were pretreated with either NAC (1 mM) or DMTU (1 mM) or CAT (300U/mL) or SOD (400U/mL) for 2 h, then treated with 500 μM 3-AIPTA for 6 h. The loss of cell viability is reflected in the loss of FDA fluorescence. (D–E) effect of ROS scavengers on ion leakage and lipid peroxidation induced by 3-AIPTA. Leaf discs of *A. thaliana* were pretreated with NAC (1 mM) or DMTU (1 mM) or CAT (300 U/mL) or SOD (400 U/mL) for 2 h, and then exposed to 500 μM 3-AIPTA for 30 h under illumination. Ion leakage and MDA were determined as described in *materials and methods*. Ion leakage reported as the ratio of 3-AIPTA-treated/control value, raw value of control is 113.03 ± 8.85 μS cm^{-1}. Data are presented as means ± SD ($n = 4$). Means denoted by the same letter did not significantly differ at $p < 0.05$.

(Fig. 7C and D) and a significant lower φ_{Ro} and RE_0/CS level (Fig. 8E and F) indicate that 3-AIPTA inhibits the reduction of the end acceptors at the PSI electron acceptor side as well as the activity of FNR. As a result, this process diverts electrons from the PSI acceptor side, that normally goes to carbon fixation path (Calvin–Benson cycle), to reduce O_2 generating $O_2^{\bullet -}$ and its decomposition product H_2O_2 [32]. Inhibition of FNR activity blocks electron transport from the reduced ferredoxin to $NADP^+$ and produces a radical which reduces oxygen to $O_2^{\bullet -}$ [9]. Taking into consideration the fact that the concentration of 500 μM 3-AIPTA, used in this study, is the concentration required to block PSII electron transport activity only by 50% [18] (Fig. 8B), we propose that 3-AIPTA-induced $O_2^{\bullet -}$ in the chloroplasts is mainly produced by PSI. This different mechanism of oxidative burst provides a reasonable explanation for the observation that 3-AIPTA kills plants with a faster rate relative to classical PSII chemical herbicides.

Fig. 9 is a summary scheme showing the sites of action of 3-AIPTA in the two pigment system and two light reaction model of photosynthesis. It also shows the sites of production of ROS. The inhibition of PSII electron flow beyond Q_A as well as the reduction of the end acceptors at the PSI electron acceptor side and the activity of FNR are suggested to be a much earlier event than chloroplast-originated ROS burst, which precedes cell injury. We conclude that 3-AIPTA-triggered cell death and leaf tissue necrosis is a direct result of oxidative damage by chloroplast-derived ROS production. This may be the common mode of action of tetramic acid families. Thus, this study contributes to the expansion of our

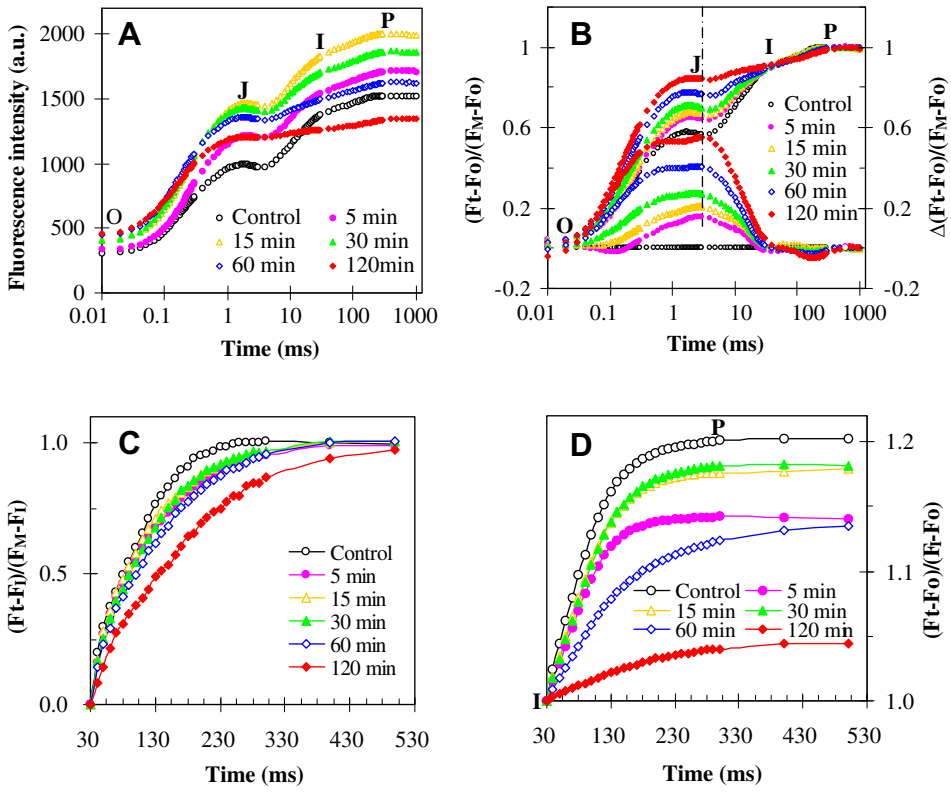

Fig. 7. Chlorophyll *a* fluorescence transients of dark-adapted epidermis-less leaf segments of *A. thaliana* treated with water (control) or 500 μM 3-AIPTA in darkness, measured with HandyPEA fluorimeter. (A) the kinetic curves plotted on a logarithmic time-scale of the raw fluorescence data are shown. (B) relative variable fluorescence between F_O and F_M: $V_t = (F_t - F_O)/(F_M - F_O)$ (the top figures); $\Delta V_t = \Delta(F_t - F_O)/(F_M - F_O)$ (the bottom figures). (C) relative variable fluorescence transient from the I to the P level ($V_{IP} = (F_t - F_I)/(F_M - F_I)$), after double normalization between the F_I and F_P points. (D) relative variable fluorescence between F_O and F_I: $V_t = (F_t - F_O)/(F_I - F_O)$. All results are the averages of about 15 independent measurements.

knowledge on 3-AIPTA and even tetramic acid as a novel photosynthesis inhibitor. In addition, it is also proposed that 3-AIPTA might be a useful new tool to study ROS in chloroplasts.

4. Materials and methods

4.1. Plant materials and chemicals

Seeds of *A. thaliana* L. (Columbia ecotype) were germinated on a mixture of soil and vermiculite (2:1 [V/V]), soaked with 1/4 strength Hoagland nutrient solution. Plants were grown in a controlled environment room at 20–25 °C under ~ 200 μmol photons m^{-2} s^{-1} white light (day/night, 8 h/16 h) and relative humidity (about 70%). After 6–8 weeks of growth, the leaves of plants were sampled.

The synthetic compound 3-AIPTA (>95%) was provided by C.L. Yang (College of Science, Nanjing Agricultural University, China). The 3-AIPTA stock solution (0.5 M) in 100% methanol was diluted in distilled water in all the experiments in this study; the final concentration of methanol was far less than 0.5% (v/v). All other chemicals used in this work were obtained from Sigma–Aldrich.

4.2. Preparation of leaf segments and treatments

The epidermis was carefully peeled from the abaxial surface of the leaves following the procedure described in reference [35]. The resulting epidermis-less leaf segments of (0.5 × 1 cm) were placed in a small Petri dish containing 10 mM MES-KCl, pH 7.2, in darkness until use. For chemical treatment, small leaf segments were transferred to fresh buffer with or without ROS scavengers NAC (1 mM), DMTU (1 mM in 0.2% DMSO), SOD (400 U/mL) or catalase (300 U/mL) for 2 h, then floated on solutions with or without 3-AIPTA with the peeled surfaces in contact with the liquid and incubated for the time indicated in each experiment, at 25 °C, under white light (100 μmol photons m^{-2} s^{-1}) in the growth chamber. After treatment, leaf segments were washed with distilled water and used for biochemical and cytological assays.

4.3. Leaf tissue damage assay

To assess lesion formation, detached-intact leaves were vacuum-infiltrated for 15 min with distilled water (control) or 500 μM 3-AIPTA and treated for 24, 48, and 72 h at 25 °C under approximately 100 μmol photons m^{-2} s^{-1} white light. After the above treatment, the samples were examined for visible lesions and this was recorded with a digital camera (Canon, SX11S, Japan). As reported in detail by Joo et al. [22], cell death was detected histochemically. Samples were briefly stained in a Trypan Blue D (TBD) mixture (30 mL ethanol, 10 g phenol, 10 mL H_2O, 10 mL glycerol, 10 mL of 10.8 M lactic acid, and 10 mg of TBD), boiled in a water bath for 3 min, and then equilibrated at room temperature (~25 °C) for 1 h. The samples were then transferred to a chloral hydrate solution (2.5 g mL^{-1}) and boiled for 10 min for destaining. The latter samples were stored and examined in 96% ethanol and recorded using a digital camera (Canon, SX11S, Japan). The experiments were repeated at least three times.

4.4. Electrolyte leakage and lipid peroxidation

To measure ion leakage [22], leaf discs of 7-mm diameter were prepared and rinsed with distilled water, then 20 pieces of leaf discs (about 0.1 g) were submerged in 5 mL of distilled water or 3-AIPTA

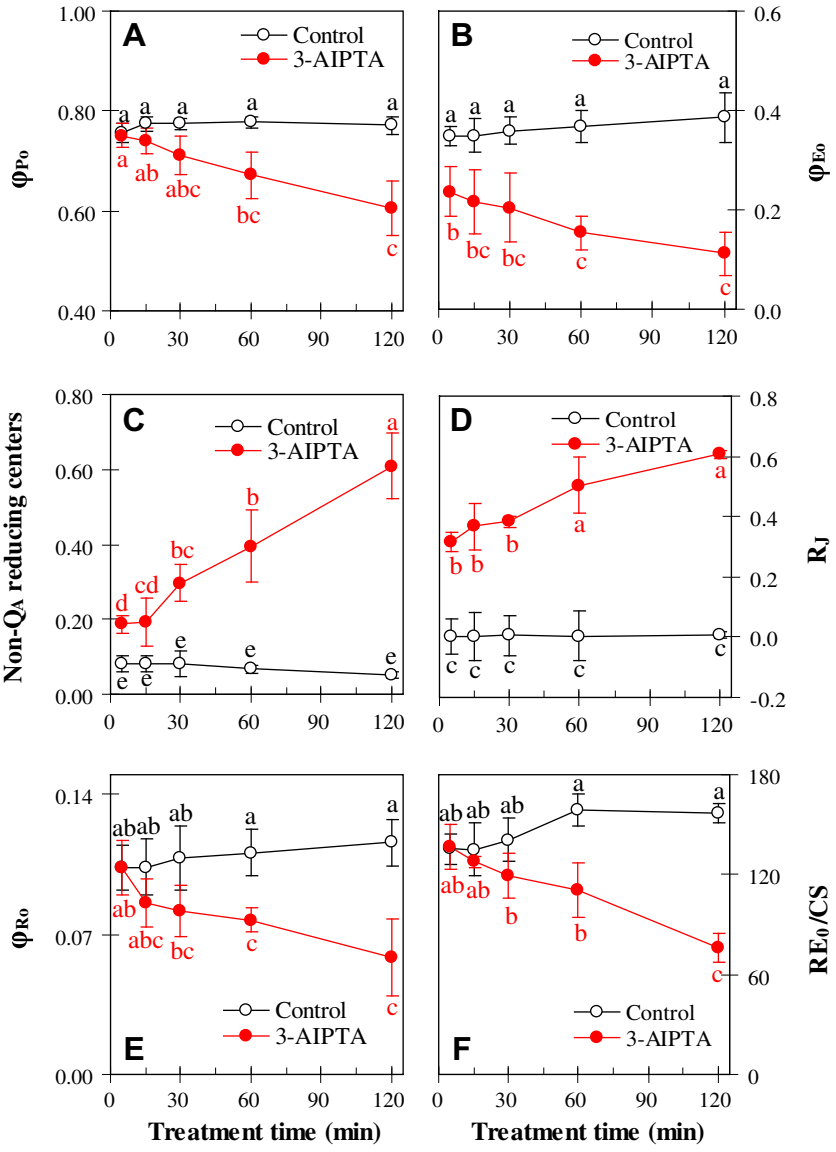

Fig. 8. Parameters quantifying the structure of the photosynthetic machinery of dark-adapted epidermis-less leaf segments of *A. thaliana* treated with water or 500 μM 3-AIPTA for different times. The maximum yield of primary photochemistry (φ_{Po}) (A), quantum yield for electron transport (φ_{Eo}) (B), non-Q_A reducing centers (C), the number of PSII RCs with Q_B-site filled with 3-AIPTA (R_J) (D), quantum yield for the reduction of the end electron acceptors at the PSI acceptor side (φ_{Ro}) (E), electron flux reducing end electron acceptors at the PSI acceptor side per CS (RE_0/CS) (F), are presented. Mean values of 15 repetitions ± SE are plotted. Different small letters indicate values significantly different within treatments ($p < 0.05$) according to the LSR test.

or bentazon solution for the indicated time with occasional agitation (25 °C, ~100 μmol (photons) m^{-2} s^{-1} white light). The conductivity of the wash solution (μS/cm) was determined using a DDS-12A conductivity meter. The total ion leakage was obtained by measuring the conductivity of the same leaf discs-containing solution, after they are autoclaved. Ion leakage per gram of wet weight was calculated by dividing the conductivity of the solution before autoclaving by the conductivity of the solution after autoclaving and then dividing the value by sample weight. Relative ion leakage is the ratio of the value obtained in treated samples to the value obtained in samples from control (water) samples at 3 h.

The level of lipid peroxidation was monitored by spectrophotometric determination of MDA, using thiobarbituric acid (TBA), according to Shimizu et al. [36] with some modifications. After treatment with or without 3-AIPTA, leaf discs (about 0.5 g) were briefly washed with distilled water to remove 3-AIPTA, and then they were homogenized in 5 mL of distilled water and stirred with a tube mixer for 1 min at room temperature. After homogenates were centrifuged at 10,000× *g* at 4 °C for 10 min, a 0.6-mL supernatant was mixed with 2.4 mL of 0.5% TBA in 20% trichloroacetic acid solution and incubated for 30 min at 95 °C. The reaction was stopped by putting the sample tubes in an ice bucket. The samples were then centrifuged at 10,000× *g* for 10 min and the absorbance of the supernatant was determined at 532 nm. The value of nonspecific light dissipation was measured at 600 nm and subtracted from that measured at 532 nm; these final extracted values represented the volume of MDAs-reactive TBA. The concentration of MDA-reactive TBA was calculated from the extinction coefficient of 155 mM^{-1} cm^{-1}.

4.5. Histochemical detection of H_2O_2 and $O_2^{\bullet-}$

H_2O_2 and $O_2^{\bullet-}$ levels were determined by in vivo staining with DAB-HCl [19] and with NBT [20] as a substrate. Briefly, *A. thaliana*

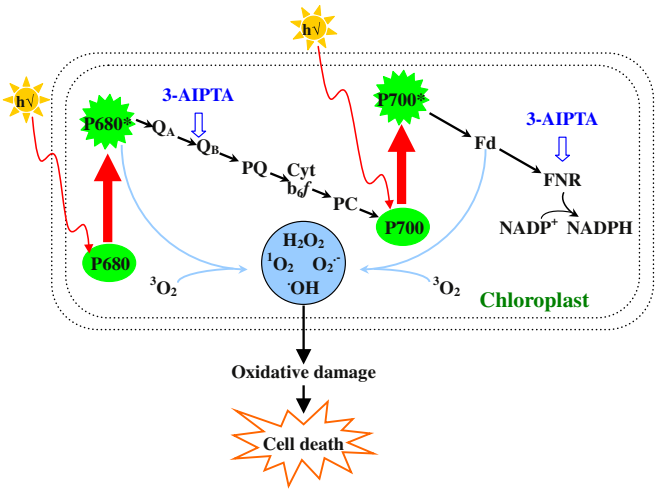

Fig. 9. A proposed model depicting 3-AIPTA-induced generation of ROS chloroplasts leading to cell death. Cyt b_6f, cytochrome; Fd, ferredoxin; FNR, ferredoxin-NADP+ reductase; H_2O_2, hydrogen peroxide; $^1O_2$, singlet oxygen; $O_2^{\bullet-}$, superoxide anion; ·OH, hydroxyl radicals; P680 and P700, PSII and PSI reaction center pigments; PC, plastocyanin; PQ, plastoquinone; Q_A and Q_B, PSII primary and secondary plastoquinone electron acceptors.

leaves were excised at the base petioles with a razor blade and then they were supplied, through the cut petioles, with a 0.1% (w/v) solution of DAB, pH 3.8 or 0.1% (w/v) NBT (dissolved in 25 mM HEPES-KOH) for 8 h under white light at 25 °C. Petioles were cut again and then placed in distilled water or 3-AIPTA or bentazon for the indicated times. After these treatments, the leaves were briefly rinsed with distilled water twice, and then decolorized by immersing the leaves in boiling ethanol (96%) for 10 min. The latter samples were stored in ethanol (96%) and photographed with a digital camera (Canon, SX11S, Japan). H_2O_2 and $O_2^{\bullet-}$ were visualized as reddish-brown and dark-blue coloration spots. The results were repeated no less than three times.

4.6. Fluorescence microscopy observation

Intracellular ROS was measured by monitoring the fluorescence of DCF, the oxidation product of H_2DCF [21]. This dye is nonfluorescent in its reduced form and readily permeates the membrane. Once in the cell, nonspecific esterases cleave acetate groups, after which the dye becomes membrane impermeable, becoming trapped inside the cells and cellular compartments. H_2DCF is converted to the fluorescent form when oxidized by H_2O_2, $O_2^{\bullet-}$ and various free radical products that are downstream from H_2O_2. After exposure to various treatments, the epidermis-less leaf segments were incubated with 10 μM H_2DCF-DA at 37 °C for 25 min in the dark. Excess H_2DCF-DA was removed with loading buffer (10 mM Tris–HCl and 50 mM KCl, pH 7.2). The samples were floated in 1 mL of the same buffer and were observed using a fluorescence microscope (Zeiss Axio Imager A1, Germany; 488 nm excitation, 525 nm emission).

Mesophyll protoplasts were isolated from the second expanded leaves from 4 to 6 week-old Arabidopsis plants, using 1% cellulase R10 and 0.2% macerozyme R10 (Yakult Honsha, Tokyo, Japan). Protoplasts were incubated in 10 μM H_2DCF-DA in W5 solution [150 mM NaCl, 125 mM $CaCl_2$, 5 mM KCl, 2 mM MES (pH5.7), and 5 mM glucose] for 15 min at 37 °C in darkness. After washing, protoplasts-preloaded with H_2DCF-DA were treated with 500 μM 3-AIPTA for the indicated times, and were observed by a laser scanning confocal microscope (Leica TCS-SPII, Germany) using the following settings: 5% power, 488 nm excitation, and 510–560 nm emission. Examination of chloroplast autofluorescence was performed using 45% power for 488 nm excitation, with 725–795 nm emission.

4.7. Assays of enzyme activity

To measure the activity of several antioxidant enzymes, the leaf segments of *A. thaliana* were treated with distilled water (control) or 500 μM 3-AIPTA for 1, 2, 4 or 6 h (25 °C, ~100 μmol photons m^{-2} s^{-1} white light). The samples (about 0.5 g) were ground in liquid nitrogen (77K) to a fine powder and were homogenized with 50 mM potassium phosphate buffer (pH 7.0) containing 1 mM ethylene diamine tetraacetic acid (EDTA) and 1% polyvinylpyrrolidone; in the case of the APX assay, 1 mM ascorbic acid was included. The homogenate was centrifuged at 15,000× *g* for 20 min at 4 °C and the supernatant was used for the following enzyme assays.

The total activity of SOD (EC1.15.1.1) was tested by monitoring the inhibition of photochemical reduction of NBT as described in reference [37]. The enzyme extracts (100 μL) were added to a 2.9 mL reaction mixture containing 50 mM potassium phosphate buffer (pH 7.8), 75 mM NBT, 13 mM methionine, 2 mM riboflavin and 0.1 mM EDTA. The reaction mixtures were illuminated for 15 min at 100 μmol photons m^{-2} s^{-1} white light. One unit of SOD activity was defined as the amount of enzyme required to decrease 50% of the reduction of NBT, as monitored at 560 nm.

CAT (EC1.11.1.6) activity was assayed by following the consumption of H_2O_2 (extinction coefficient, 39.4 mM^{-1} cm^{-1}) at 240 nm for 3 min [38]. The reaction mixture (3 mL) contained 50 mM potassium phosphate buffer (pH 7.0), 200 μL enzyme extracts and 10 mM H_2O_2.

APX (EC1.11.1.11) activity was measured by following decrease of absorbance at 290 nm, A_{290} (extinction coefficient, 2.8 mM^{-1} cm^{-1}) for the first 3 min in a 1-mL reaction mixture containing 50 mM potassium phosphate buffer (pH 7.0), 200 μL enzyme extract(s), 0.5 mM ascorbate (ASC) and 0.1 mM H_2O_2. Correction was made for the low, non-enzymatic oxidation of ASC by H_2O_2 [39].

4.8. Cell viability

After treatment with distilled water or 3-AIPTA or bentazon, leaf segments of *A. thaliana* were incubated with 0.01% FDA for 10 min at 20 °C in darkness. FDA fluorescence was observed using fluorescence microscopy (Zeiss Axio Imager A1, 495 nm excitation and 500–550 nm emission) [40]. FDA fluorescence decreases as the dye leaks from the dead cells.

4.9. Chlorophyll *a* fluorescence transient

The epidermis-less leaf segments were submerged in distilled water or 3-AIPTA solution, and then incubated for the indicated time at 25 °C in complete darkness. Chl *a* fluorescence transient (induction) was measured at room temperature with a HandyPEA fluorometer (Hansatech, UK). The experiment was repeated at least three times with five repetitions per treatment. The OJIP fluorescence transients were induced by 1 s pulses of red light (650 nm, 3500 μmol photons m^{-2} s^{-1}); this provided valuable information on the photosynthetic activities and physiological vitality. We note that O refers to the initial minimal fluorescence level; P (500 ms – 1 s) is for the peak and J (2 ms) and I (30 ms) are inflection points between the O and the P levels. The rise in Chl *a* fluorescence, the OJIP transient, was analysed according to the so-called JIP-test [23,24]. The JIP-test defines the maximal (subscript "o" indicates that the parameter refers to the onset of

illumination) energy fluxes in the energy cascade for the following events: Absorption (ABS), Trapping (TR_0), Electron Transport (ET_0), Reduction of End acceptors of PSI (RE_0), and leaf Cross Section (CS). For calculation of the values of the above parameters, the following data were utilized: the initial fluorescence F_O, measured at 20 μs (O-step): at this time all reaction centers (RCs) are open; fluorescence intensity F_J at 2 ms (J-step); fluorescence intensity F_I at 30 ms (I-step); the maximal fluorescence intensity F_M ; this is equal to F_P, since the pulse used was saturating, i.e., all the Q_A is reduced (all RCs are closed).

Other parameters were:

- Relative variable fluorescence V_t, defined as $(F_t-F_O)/(F_M-F_O)$; thus, $V_J = (F_J-F_O)/(F_M-F_O)$, $V_I = (F_I-F_O)/(F_M-F_O)$.
- The maximum quantum yield of primary photochemistry, φ_{Po}, defined as $TR_0/ABS = 1-(F_O/F_M)$.
- The probability that an electron moves further than Q_A^- (ψ_{Eo}), defined as $ET_0/TR_0 = (1-V_J)$.
- The maximum yield of electron transport (φ_{Eo}) as $ET_0/ABS = [1-(F_O/F_M)].(1-V_J)$.
- The amount of Q_A-reducing centers of the reference samples are calculated as: Q_A-reducing centers $= (RC/RC_{ref.}).(ABS/ABS_{ref.}) = [(RC/CS)/(RC/CS)_{ref.}].[(ABS/CS)/(ABS/CS)_{ref.}]$; therefore, the fraction of non-Q_A reducing centers $= 1-Q_A$-reducing centers $= 1-(RC/RC_{ref.}).(ABS/ABS_{ref.})$.
- The parameter R_J, an expression for the number of RCII with Q_B-site filled by PSII inhibitor: $R_J = [V_J-(V_J)_{control}]/[1-(V_J)_{control}] = 1-(\psi_{Eo}'/\psi_{Eo(ref)})$.
- The quantum yield for the reduction of the end electron acceptors at the PSI acceptor side $(\varphi_{Ro}) = RE_0/ABS = \varphi_{Po}.\psi_{Eo}.\delta_{Ro} = \varphi_{Po}.(1-V_I)$.
- The probability of reductions at the PSI electron acceptor side per excited cross section (CS): $RE_0/CS = \delta_{Ro}.(ET_0/CS)$
- $\delta_{Ro} = RE_0/ET_0 = (1-V_I)/(1-V_J)$, which expresses the probability that an electron is transported from the reduced intersystem electron acceptors to final electron acceptors of PSI.

4.10. Statistical analysis

Relative results were analyzed with STATGRAPHICS PLUS software Ver.2.1 (Manugistics, Rockville, MD, USA). One-way ANOVA was carried out and means were separated using Duncan's least significant ranges (LSR) at 95%. Each experiment was repeated three times with at least three replicates per treatment.

Acknowledgements

This work was supported by the National Natural Science Foundation of China (31000834), New Teacher Foundation of Doctoral Program of Education Ministry of China (200803071004), Doctoral Program of Education Ministry of China (200900 97110018), China 863 Program (2011AA10A206), 111 Project (B07030) and Project Funded by the Priority Academic Program Development of Jiangsu Higher Education Institutions. We thank Bruce Auld (Charles Sturt University, Australia) for suggestions for improvements in the manuscript. We refer the readers to a very recent highly relevant review by Danon (2012) on oxidative stress and signalling [41].

Appendix. Supplementary data

Supplementary data associated with this article can be found, in the online version, at doi:10.1016/j.plaphy.2011.11.004.

References

[1] M. Brosché, S. Kangasjärvi, K. Overmyer, M. Wrzazek, J. .Kangasjärvi, Stress signalling III: reactive oxygen species. in: A. Pareek, S.K. Sopory, H.J. Bohnert, Govindjee (Eds.), Abiotic Stress Adaptation in Plants. Springer, Dordrecht, 2010, pp. 91–102.
[2] K. Apel, H. Hirt, Reactive oxygen species: metabolism, oxidative stress, and signal transduction, Annu. Rev. Plant Biol. 55 (2004) 373–399.
[3] A. Das, M. Kawai-Yamada, H. Uchimiya, Programmed cell death in plants. in: A. Pareek, S.K. Sopory, H.J. Bohnert, Govindjee (Eds.), Abiotic Stress Adaptation in Plants. Springer, Dordrecht, 2010, pp. 371–386.
[4] K. Asada, Production and scavenging of reactive oxygen species in chloroplasts and their functions, Plant Physiol. 141 (2006) 391–396.
[5] C. Laloi, K. Apel, A. Danon, Reactive oxygen signaling: the latest news, Curr. Opin. Plant Biol. 7 (2004) 323–328.
[6] Z. Suntres, Role of antioxidants in paraquat toxicity, Toxicology 180 (2002) 65–77.
[7] C.F. Babbs, J.A. Pham, R.C. Coolbaugh, Lethal hydroxyl radical production in paraquat-treated plants, Plant Physiol. 90 (1989) 1267–1270.
[8] B. Förster, C.B. Osmond, B.J. Pogson, Improved survival of very high light and oxidative stress is conferred by spontaneous gain-of-function mutations in *Chlamydomonas*, Biochim. Biophys. Acta 1709 (2005) 45–57.
[9] B. Halliwell, Oxygen radicals: their formation in plant tissues and their role in herbicide damage. in: N.R. Baker, M.P. Percival (Eds.), Herbicides. Elsevier Science, Amsterdam-London-New York-Tokyo, 1991, pp. 87–129.
[10] F.D. Hess, Light-dependent herbicides: an overview, Weed Sci. 48 (2000) 160–170.
[11] R. Schobert, A. Schlenk, Tetramic and tetronic acids: an update on new derivatives and biological aspects, Bioorgan. Med. Chem. 16 (2008) 4203–4221.
[12] R. Fischer, T. Bretschneider, H.J. Santel, K. Lürrsen, R.R. Schmidt, C. Erdelen, Herbicidal and insecticidal 3-benzoyl-prrrolidin-2,4-dion-derivates (1994) WO9401401.
[13] R. Fischer, S. Lehr, D. Feucht, P. Löesel, O. Malsam, G. Bojak, T. Auler, M.J. Hills, H. Kehne, C.H. Rosinger, 2-ethyl-4,6-dimethyl-phenyl-substituted tetramic acid derivates as pest control agents and/or herbicides (2005) WO2005048710.
[14] B.J.L. Royles, Naturally occurring tetramic acid: structure, isolation, and synthesis, Chem. Rev. 95 (1995) 1981–2001.
[15] S.G. Chen, X.M. Xu, X.B. Dai, C.L. Yang, S. Qiang, Identification of tenuazonic acid as a novel type of natural photosystem II inhibitor binding in Q_B-site of *Chlamydomonas reinhardtii*, Biochim. Biophys. Acta 1767 (2007) 306–318.
[16] S.G. Chen, C.Y. Ying, S. Qiang, F.Y. Zhou, X.B. Dai, Chloroplastic oxidative burst induced by tenuazonic acid, a natural photosynthesis inhibitor, triggers cell necrosis in *Eupatorium adenophorum* Spreng, Biochim. Biophys. Acta 1797 (2010) 391–405.
[17] S. Gatenbeck, J. Sierankiewicz, Microbial production of tenuazonic acid analogues, Antimicrob. Agents Chemother. 3 (1973) 308–309.
[18] S.G. Chen, F.Y. Zhou, C.Y. Yin, R.J. Strasser, C.L. Yang, S. Qiang, Application of fast chlorophyll a fluorescence kinetics to probe action target of 3-acetyl-5-isopropyltetramic acid, Environ. Exp. Bot. 71 (2011) 269–279.
[19] M. Orozco-Cardenas, C.A. Ryan, Hydrogen peroxide is generated systemically in plant leaves by wounding and systemin via the octadecanoid pathway, Proc. Natl. Acad. Sci. USA 96 (1999) 6553–6557.
[20] J.A. Hernández, M.A. Ferrer, A. Jiménez, A.R. Barceló, F. Sevilla, Antioxidant systems and O_2^-/H_2O_2 production in the apoplast of pea leaves. Its relation with salt-induced necrotic in minor veins, Plant Physiol. 127 (2001) 817–831.
[21] A. Allan, R. Fluhr, Two distinct sources of elicited reactive oxygen species in tobacco epidermal cells, Plant Cell 9 (1997) 1559–1572.
[22] J.H. Joo, S.Y. Wang, J.G. Chen, A.M. Jones, N.V. Fedoroff, Different signaling and cell death roles of heterotrimeric G protein α and β subunits in the *Arabidopsis* oxidative stress responsed to ozone, Plant Cell 17 (2005) 957–970.
[23] R.J. Strasser, M. Tsimilli-Michael, A. Srivastava, Analysis of the chlorophyll a fluorescence transient. in: G.C. Papageorgiou, Govindjee (Eds.), Chlorophyll Fluorescence: a Signature of Photosynthesis. Kluwer Academic Publishers Press, Netherlands, 2004, pp. 321–362.
[24] A. Stirbet, Govindjee, On the relation between the Kautsky effect (chlorophyll *a* fluorescence induction) and Photosystem II: basics and applications of the OJIP fluorescence transient, J. Photochem. Photobiol. B. Biol. 104 (2011) 236–257.
[25] G. Schansker, S.Z. Tóth, R.J. Strasser, Methylviolegen and dibromothymoquinone treatments of pea leaves reveal the role of photosystem I in the Chl *a* fluorescence rise OJIP, Biochim. Biophys. Acta 1706 (2005) 250–261.
[26] J.L. Gunsolus, W.S. Curran, Herbicide Mode of Action and Injury Symptoms 377. University of Minnesota Extension Service, North Central Regional Publication, 1999, Available at:. http://www.extension.umn.edu.
[27] A.W. Rutherford, A. Krieger-Liszkay, Herbicide-induced oxidative stress in photosystem II, Trends Biochem. Sci. 26 (2001) 648–653.
[28] C. Fufezan, A.W. Rutherford, A. Krieger-Liszkay, Singlet oxygen production in herbicide-treated photosystem II, FEBS Lett. 532 (2002) 407–410.
[29] J.G. Scandalios, The rise of ROS, Trends Biochem. Sci. 27 (2002) 483–486.
[30] J.M. Mach, J.T. Greenberg, Free radicals and oxidative stress. in: L.D. Noodén (Ed.), Plant Cell Death Processes. Elsevier Academic Press, Amsterdam-Boston, 2004, pp. 203–214.

[31] J.R. Anthony, K.L. Warczak, T.J. Donohue, A transcriptional response to singlet oxygen, a toxic byproduct of photosynthesis, Proc. Natl. Acad. Sci. USA 102 (2005) 6502–6507.
[32] B. Hock, E.F. Elstner, Plant Toxicology, fourth ed.. Marcel Dekker Press, New York, 2005.
[33] P. Pospíšil, Production of reactive oxygen species by photosystem II, Biochim. Biophys. Acta 1787 (2009) 1151–1160.
[34] A.H. Mehler, Studies on reactions of illuminated chloroplasts. I. Mechanism of the reduction of oxygen and other hill reagents, Arch. Biochem. Biophys. 33 (1951) 65–77.
[35] N. Yao, Y. Tada, P. Park, H. Nakayashiki, Y. Tosa, S. Mayama, Novel evidence for apoptotic cell response and differential signals in chromatin condensation and DNA cleavage in victorin-treated oats, Plant J. 28 (2001) 13–26.
[36] N. Shimizu, N. Hosogi, G.S. Hyon, S. Jiang, K. Inoue, P. Park, Reactive oxygen species (ROS) generation and ROS-induced lipid peroxidation are associated with plasma membrane modifications in host cells in response to AK-toxin I from *Alternaria alternata* Japanese pear pathotype, J. Gen. Plant Pathol. 72 (2006) 6–15.
[37] C.N. Giannopolitis, S.K. Ries, Superoxide dismutases: I. occurrence in higher plants, Plant Physiol. 59 (1977) 309–314.
[38] H. Aebi, Catalase in vitro, Methods Enzymol. 105 (1984) 121–126.
[39] Y. Nakano, K. Asada, Hydrogen peroxide is scavenged by ascorbate-specific peroxidase in spinach chloroplasts, Plant Cell Physiol. 22 (1981) 867–880.
[40] H.P. Bais, R. Vepachedu, S. Gilroy, R.M. Callaway, J.M. Vivanco, Allelopathy and exotic plant invasion: from molecules and genes to species interactions, Science 301 (2003) 1377–1380.
[41] A. Danon, Environmentally-induced stress and its signaling. in: J.J. Eaton-Rye, B.C. Tripathy, T.D. Sharkey (Eds.), Photosynthesis: Plastid Biology, Energy Conversion and Carbon Assimilation, Advances in Photosynthesis and Respiration, Volume 34. Springer, Dordrecht, 2012, pp. 319–330.